Biomaterials 30 (2009) 2425–2432

Contents lists available at ScienceDirect

Biomaterials

journal homepage: www.elsevier.com/locate/biomaterials

Microscale mechanical properties of single elastic fibers: The role of fibrillin–microfibrils

Mieke M.J.F. Koenders [a,1], Lanti Yang [b,1], Ronnie G. Wismans [a], Kees O. van der Werf [c], Dieter P. Reinhardt [d], Willeke Daamen [a], Martin L. Bennink [c], Pieter J. Dijkstra [b], Toin H. van Kuppevelt [a], Jan Feijen [b,*]

[a] Department of Biochemistry, Nijmegen Center for Molecular Life Sciences, University Nijmegen Medical Center, Nijmegen, The Netherlands
[b] Department of Polymer Chemistry and Biomaterials, Faculty of Science & Technology and Institute for Biomedical Technology (BMTI), University of Twente, Enschede, The Netherlands
[c] Department of Biophysical Engineering, Faculty of Science & Technology and MESA+ Institute for Nanotechnology, University of Twente, Enschede, The Netherlands
[d] Department of Anatomy and Cell Biology and Faculty of Dentistry, McGill University, Montreal, Canada

ARTICLE INFO

Article history:
Received 20 November 2008
Accepted 22 January 2009
Available online 13 February 2009

Keywords:
AFM (atomic force microscopy)
Elastin
Mechanical properties
Mechanical test
Nano-indentation

ABSTRACT

Micromechanical properties of single elastic fibers and fibrillin–microfibrils, isolated from equine *ligamentum nuchae* using chemical and enzymatic methods, were determined with atomic force microscopy (AFM). Young's moduli of single elastic fibers immersed in water, devoid of or containing fibrillin–microfibrils, were determined using bending tests. Bending freely suspended elastic fibers on a micro-channeled substrate by a tip-less AFM cantilever generated a force versus displacement curve from which Young's moduli were calculated. For single elastic fibers, Young's moduli in the range of 0.3–1.5 MPa were determined, values not significantly affected by the presence of fibrillin–microfibrils. To further understand the role of fibrillin–microfibrils in vertebrate elastic fibers, layers of fibrillin–microfibrils were subjected to nano-indentation tests. From the slope of the force versus indentation curves, Young's moduli ranging between 0.56 and 0.74 MPa were calculated. The results suggest that fibrillin–microfibrils are not essential for the mechanical properties of single vertebrate elastic fibers.

1. Introduction

Elastic fibers are essential structures which endow resilience to the extracellular matrix (ECM) by a passive, entropy-driven mechanism allowing stretching and recoil [1]. In vertebrates, the elasticity of several tissues and organs such as blood vessels, skin, lung, muscle, ligaments and cartilage [2–4] is provided by elastic fibers. Using macro-mechanical testing, the elasticity of elastic fiber-rich tissues has been a subject of study for years. Young's modulus of elastic fiber-rich tissue samples of purified dog or sheep aorta was determined to be in the range of 0.13–0.65 MPa [5]. Young's moduli between 0.1 and 0.8 MPa were calculated for tissue samples of purified pig aorta enriched with elastic fibers [6]. Young's modulus of single elastic fibers isolated from bovine *ligamentum nuchae* was, for the first time, determined by Aaron et al. [7] using a microtest apparatus attached to a polarizing microscope and was in the range of 0.4–1.2 MPa. The vertebrate elastic fibers contain at least two morphological components: amorphous elastin, which accounts for 90% of the elastic fibers, and microfibrils, which are 10–12 nm in diameter [1,8]. Fibrillin-1 is the major component of the microfibrils [3], although other, less abundant, molecules like microfibril-associated glycoproteins (MAGPs) [9–11], emilins [12–14], and latent transforming growth factor-β binding proteins (LTBPs) [15–17] have been identified.

Fibrillin–microfibrils are considered necessary for the assembly of a functional elastic fiber. During elastic fiber formation, fibrillin–microfibrils appear first and serve as a scaffold for the deposition of tropo-elastin [8]. Invertebrates lack elastin, and the essential elastic recoil of their tissue can only be provided by fibrillin–microfibrils, suggesting that fibrillin–microfibrils are elastic [18–20]. Young's modulus of the invertebrate microfibrillar network is in the range of 0.2–1.1 MPa [19–21]. The question arises as to whether vertebrate fibrillin–microfibrils also have similar mechanical properties and play a role in the mechanical properties of vertebrate organs and elastic fibers. Work on mammalian ciliary zonular filaments, a structure solely composed of fibrillin–microfibrils, gave insight into the mechanical properties of vertebrate fibrillin–microfibrils. X-ray diffraction and biomechanical testing of zonular filaments indicated that fibrillin–microfibrils have Young's moduli in the range of 0.19–1.88 MPa, similar in magnitude to invertebrates fibrillin–microfibrils and elastic fibers [22–24]. However, using

* Corresponding author. Tel.: +31 53 4892968.
E-mail address: j.feijen@utwente.nl (J. Feijen).
[1] Authors contributed equally.

0142-9612/$ – see front matter © 2009 Elsevier Ltd. All rights reserved.
doi:10.1016/j.biomaterials.2009.01.038

molecular combing, Young's moduli of single fibrillin–microfibrils from zonular filaments was estimated to be 78–96 MPa, which are two orders of magnitude higher than the modulus determined from tissue samples [25]. From these data, the authors suggested that fibrillin–microfibrils play a role in reinforcing the vertebrate elastic fibers. Recent work by Lillie et al. also indicated that removal of fibrillin–microfibrils from the elastic fibers of porcine aorta results in a slightly decreased Young's modulus at low strain and a slightly increased modulus at high strain [6]. To date, there is debate on how fibrillin–microfibrils contribute to the mechanical properties of elastic fibers and in what order of magnitude Young's modulus of fibrillin–microfibrils ranges.

Since elastin is one of the most abundant proteins in human tissues, elastic fibers are regarded as highly suitable scaffolding material for tissue engineering applications. For the use of elastic fibers as a biomaterial, purity of the material is an important issue. Contamination with proteins may lead to unwanted immunological reactions. Efforts have been made to use purified intact elastic fibers as scaffolds in tissue engineering [26–29]. From the work of Daamen et al., it is suggested that purified intact elastic fibers devoid of fibrillin–microfibrils are preferred for scaffold purposes [29]. The mechanical properties of the purified elastic fibers, devoid of or containing fibrillin–microfibrils, should also be determined for an adequate use of these fibers in tissue engineering.

This study reports on the biomechanical properties of single purified elastic fibers. Highly purified elastic fibers, devoid of or containing fibrillin–microfibrils, were successfully extracted from equine *ligamentum nuchae* and measured with an atomic force microscope (AFM). Micromechanical bending tests, similarly as previously described [30], were for the first time performed on single elastic fibers to determine Young's moduli of the fibers. Young's modulus of fibrillin–microfibrils was determined using AFM-based nano-indentation. The contribution of fibrillin–microfibrils to the mechanical properties of the vertebrate single elastic fibers was evaluated using the combined results from bending and nano-indentation experiments.

2. Materials and methods

All experimental procedures were performed at room temperature, unless stated otherwise.

2.1. Isolation of elastic fibers

Elastic fibers, devoid of or containing fibrillin–microfibrils, were isolated from equine *ligamentum nuchae* using a modification of previously published work of Daamen et al. [31,32]. *Ligamentum nuchae* was pulverized under liquid nitrogen conditions using a pulverisette with a 1 mm sieve (Fritsch pulverisette 19, Idar-Oberstein, Germany). The pulverized tissue was subjected three times to an overnight extraction with 10 vol. (10 ml/g) of 1 M NaCl containing 0.02% (w/v) NaN_3 at 4 °C. After each extraction step, insoluble material was recovered by centrifugation at 5000 × *g* at 4 °C for 20 min. After the last extraction step, the pellet was washed with demineralised water and resuspended in 10 vol. of ethanol. After 90 min, the suspension was filtered through a paper funnel. This procedure was repeated with 10 vol. of chloroform/methanol (2:1) for 90 min, 10 vol. of acetone for 30 min, and 10 vol. of ether for 30 min. The resulting residue was dried in a desiccator. The dried material was extracted with 15 vol. of 97% formic acid with 1% (w/v) cyanogen bromide for 24 h under non-oxidizing conditions. After extraction, the suspension was diluted with 45 vol. of demineralised water and centrifuged at 5000 × *g* at 4 °C for 15 min. The pellet was washed with demineralised water until a pH of 6–7 was reached. After washing, the pellet was resuspended in 10 vol. of demineralised water and this suspension was divided in two parts. One half of the suspension was used to isolate elastic fibers devoid of fibrillin–microfibrils (Method I) and the other half was used to isolate elastic fibers containing fibrillin–microfibrils (Method II).

2.1.1. Method I

After centrifugation, the pellet was resuspended in 5 vol. of 0.5 M Tris–HCl pH 6.8 containing 4 M urea, 1 M β-mercaptoethanol, and 0.02% (w/v) NaN_3 and incubated overnight. This extraction step was repeated three times and after each step insoluble material was recovered by centrifugation at 5000 × *g* at 4 °C for 20 min. The resulting pellet was washed for 6 times with 5 vol. of demineralised water. After centrifugation, the pellet was resuspended in 5 vol. 0.1 M NH_4HCO_3, pH 8.2 containing 0.02% (w/v) NaN_3 and 10,000 U trypsin (T-4665, Sigma, St. Louis, USA) and incubated for 4 h at 37 °C. The suspension was centrifuged and the pellet was washed with demineralised water, followed by 3 overnight extractions with 5 vol. 1 M NaCl containing 0.02% (w/v) NaN_3. The resulting pellet was washed with demineralised water and the end product was stored at −80 °C.

2.1.2. Method II

After centrifugation, the pellet was resuspended in 5 vol. 0.2 M Tris–HCl pH 7.4 containing 0.05 M $CaCl_2$, 0.02% (w/v) NaN_3, and 500 U collagenase type VII (Sigma) and incubated for 4 h at 37 °C. The suspension was centrifuged and the pellet was washed with demineralised water, followed by 3 overnight extractions with 5 vol. 1 M NaCl containing 0.02% (w/v) NaN_3. The resulting pellet was washed with demineralised water and the end product was stored at −80 °C.

2.2. Purity assessment

2.2.1. Gel electrophoresis

Elastic fiber preparations were analyzed under reducing conditions (5% β-mercaptoethanol) on a 10% (w/v) polyacrylamide gel. Proteins were visualized by silver staining using a 0.1% (w/v) $AgNO_3$ solution.

2.2.2. Transmission Electron Microscopy (TEM)

Elastic fiber preparations were embedded in 1.5% (w/v) agarose, fixed in 2% (v/v) glutaraldehyde in 0.1 M phosphate buffer pH 7.4, post fixed with 1% (w/v) osmium tetroxide, dehydrated in ascending series of ethanol, and embedded in epon 812. Ultrathin sections (60 nm) were picked up on formvar-coated grids, post-stained with lead citrate and uranyl acetate, and subsequently imaged using electron microscopy (JEOL 1010, Tokyo, Japan).

2.2.3. Scanning Electron Microscopy (SEM)

Lyophilized elastic fiber preparations were mounted on stubs and sputtered with an ultrathin layer of gold in a polaron E5100 SEM coating system. Specimens were studied with an SEM apparatus (JEOL JSM-6310, Tokyo, Japan) operating at 15 kV.

2.2.4. Immune Fluorescence Assay (IFA)

Elastic fiber preparations were suspended in demineralised water and frozen in liquid nitrogen. 4 μm cryosections were cut and incubated in 1% (w/v) bovine serum albumin (BSA, fraction V, Sigma) in PBS to block aspecific binding sites. Sections were incubated overnight at 4 °C with rabbit anti-bovine type I collagen (1:50, Chemicon, Temecula, USA), rabbit anti-human fibrillin-1 (1:500, a kind gift of Dr. Dieter Reinhardt [33], and mouse anti-bovine elastin (1:500, clone BA-4, Sigma) diluted in PBS containing 1% (w/v) BSA. After washing with PBS, bound antibody was detected with 1:100 diluted goat anti-mouse IgG Alexa 488 or goat anti-rabbit IgG Alexa 488 (Molecular Probes, Eugene, USA) in PBS containing 1% (w/v) BSA for 90 min. Sections were washed in PBS and mounted in mowiol (4-88, Calbiochem, La Jolla, USA).

2.3. Micromechanical bending tests of elastic fibers using AFM

Quartz glass substrates with parallel micro-channels were prepared by reactive ion etching using an RIE Elektrotech system (Elektrotech Twin PF 340, UK). The width and depth of the channels were determined by AFM (home-built instrument) and SEM (LEO Gemini 1550 FEG-SEM, Oberkochen, Germany) measurements.

Diluted suspensions of elastic fiber preparations, devoid of or containing fibrillin–microfibrils, were prepared by adding 15 mg of preparation I or II to 20 ml demineralised water. Glass substrates were incubated in the diluted suspension for 10 min, and dried overnight.

A home-built AFM combined with an optical microscope was used for micromechanical bending tests. Bending experiments were performed using modified triangular silicon nitride cantilevers (coated sharp microlevers MSCT-AUHW, type F, spring constant $k = 0.5$ N/m, Veeco, Cambridge, UK). The tip of the AFM cantilever was removed using a focused ion beam (FIB) (FEI, Nova Nanolab 600 dual beam machine, Eindhoven, the Netherlands), which facilitated the positioning of the cantilever above the fiber, because the width of the cantilever was slightly wider than the fiber diameter. The spring constant of each tip-less cantilever was calibrated by pushing on a pre-calibrated cantilever as described elsewhere [34]. Before starting the measurement, the glass substrate containing the elastic fibers was immersed in 1 ml demineralised water and left to equilibrate for 15 min. Micromechanical bending tests were performed by bending the elastic fiber at the middle point of the channel using an AFM cantilever. Deflections versus piezo displacement curves were directly obtained from the micromechanical bending tests. From the results, forces versus displacement curves were derived to estimate Young's modulus of single elastic fibers. Local indentation of elastic fibers during bending was estimated by indenting the same fiber located on the glass surface.

2.4. Diameter of the elastic fibers in water

The diameter of the elastic fibers used in the micromechanical bending tests was determined by Scanning Electron Microscopy (SEM) (LEO Gemini 1550 FEG-SEM,). The diameter of an elastic fiber in water was estimated from SEM images made with an environmental SEM system (Philips XL 30 ESEM-FEG, Eindhoven, the Netherlands) at water pressure of 5.4 Torr and temperature of 5 °C.

2.5. Isolation of fibrillin–microfibrils

Fibrillin–microfibrils were isolated from equine *ligamentum nuchae* as described [35]. Briefly, tissue was dissected into small pieces and incubated in 50 mM Tris–HCl pH 7.4 containing 0.4 M NaCl, 10 mM $CaCl_2$, type Ia collagenase (Sigma, St. Louis, MO, USA), 2 mM phenylmethylsulphonyl fluoride (PMSF), and 5 mM *N*-ethylmaleimide (NEM) for 18 h. Samples were centrifuged at 5000 × *g* at 4 °C for 5 min and the supernatant was size fractionated on a sepharose CL-4B column (Amersham, Piscataway, USA) in 20 mM Tris–HCl pH 7.4 containing 0.4 M NaCl and 2 mM $CaCl_2$ using a flow rate of 0.2 ml/min. The void volume contained fibrillin–microfibrils, as detected by dot–blot immunochemistry with rabbit anti-fibrillin-1 (1:500).

2.6. Imaging of fibrillin–microfibrils using AFM

The void volume, containing fibrillin–microfibrils, was diluted 10 times in water. The diluted suspension of fibrillin–microfibrils was brought onto a cleaned glass substrate. After drying, the glass substrate was washed with demineralised water in order to remove any unattached material. The fibrillin–microfibrils were imaged by tapping mode in air using a home-built AFM system with V-shaped Si_3N_4 cantilevers (coated sharp microlevers MSCT-AUHW, type F, spring constant $k = 0.5$ N/m, Veeco, Cambridge, UK). A tapping frequency of ~120 kHz and a tapping amplitude of ~400–600 nm were used.

2.7. Nano-indentation of fibrillin–microfibrils using AFM

A suspension of fibrillin–microfibrils from the non-diluted void volume was brought onto a cleaned glass substrate to obtain multi-layers of fibrillin–microfibrils. After drying and washing with demineralised water, the fibrillin–microfibrils layers were imaged using AFM, as described above to obtain information on the morphology of the microfibrils. Using an initial large-scale image, the desired area for indentation was selected. Before starting the measurements, the glass substrate containing the fibrillin–microfibrils was immersed in 1 ml demineralised water and left to equilibrate for 15 min. Nano-indentation was performed at different locations on the surface using the V-shaped Si_3N_4 cantilevers (coated sharp microlevers MSCT-AUHW, type C, spring constant $k = 0.01$ N/m, Veeco, Cambridge, UK) applying an AFM piezo displacement of 500 nm and a frequency of 10 Hz. The spring constant of each cantilever was calibrated by pushing on a pre-calibrated cantilever as described elsewhere [34]. To obtain a force versus indentation curve, the sensitivity (S) of the applied method, i.e. the ratio between the bending of the cantilever and the deflection as measured by the quadrant detector, was derived from the force versus displacement curve using a glass surface. Young's modulus of fibrillin–microfibrils was calculated from the force versus indentation curve.

3. Results and discussion

3.1. Elastic fiber preparations

To visualize major contaminations (e.g. globular proteins), purified elastic fiber preparations, devoid of or containing fibrillin–microfibrils, were subjected to gel electrophoresis. Contaminants and elastin degradation products are soluble and will penetrate the gel, whereas the insoluble elastic fiber preparations will not. The consecutive extraction steps and the specific enzyme digestion used in methods I and II successfully removed contaminants from the starting material, as indicated by the absence of protein bands (Fig. 1A, lanes 2 and 4). Moreover, no signs of degradation products of elastin were present. Similarly, scanning electron microscopy (SEM) revealed intact elastic fibers with a smooth surface (Fig. 1B and C).

Transmission electron microscopy (TEM) and immunostainings were applied to detect collagen, fibrillin-1 containing microfibrils, and elastin in the elastic fiber preparations. Staining for elastin in elastic fiber preparations devoid of fibrillin–microfibrils (Method I) was abundant, whereas staining for type I collagen and fibrillin-1 was absent (Fig. 2A and B for elastin and fibrillin-1). Elastic fiber preparations containing fibrillin–microfibrils (Method II) displayed abundant elastin and fibrillin-1 staining (Fig. 2D and E). Type I collagen was absent (data not displayed). Abundant black dots/filamentous structures, indicative for fibrillin–microfibrils, were found only in the TEM images of elastic fibers containing fibrillin–microfibrils (Fig. 2F), which was in line with the results obtained by immunostainings. In conclusion, two elastic fiber preparations were prepared, one preparation contained pure, intact elastic fibers devoid of fibrillin–microfibrils (Method I) and the other preparation contained pure, intact elastic fibers containing fibrillin–microfibrils (Method II). However, it cannot be excluded that the isolation protocols used may have affected the components to some extent.

3.2. Mechanical properties of single elastic fibers

Reactive ion etching was used to prepare the glass substrates with well defined micro-channels with a width of 5 μm–10 μm and a depth of 600 nm. After incubating the glass substrates with the diluted elastic fiber preparations, single elastic fibers spanning the micro-channels were selected for micromechanical AFM bending tests using an inverted optical microscope. SEM images clearly showed that the single elastic fibers were spanning the micro-channels of the glass substrate (Fig. 3A). These fibers were bent with a tip-less cantilever along the fiber axis. With the piezo movement versus deflection curves obtained directly from the AFM bending data, the force (F) and the displacement (z) in the z-direction were calculated using the following equations:

$$z = A - D \times S \tag{1}$$

$$F = D \times S \times k \tag{2}$$

in which A is the piezo movement in the z-direction, D is the deflection measured (in Volts), S is the sensitivity of the cantilever, and k is the calibrated spring constant of the cantilever. A force versus displacement curve was obtained by plotting displacement (z) on the x-axis and force (F) on the y-axis.

By exerting a force on the elastic fibers at the middle point of the channel, a displacement from bending was induced as well as a local indentation of the fiber. In order to determine the modulus of an elastic fiber by bending tests, the displacement has to be corrected for this indentation. Local indentation can be determined from the force versus displacement curve of indenting an elastic fiber supported on the glass surface (indentation curve in Fig. 3B). By subtracting for each force the displacement resulting from only indentation from the total displacement as obtained by measuring at the middle point (bending curve in Fig. 3B), the displacement only resulting from the bending can be obtained (Fig. 3C).

A linear force versus displacement curve was found for bending elastic fibers devoid of or containing fibrillin–microfibrils (Fig. 3C). In the experiments, no significant difference was found in the force versus displacement curve after bending the fiber at the same position multiple times, which ensured the reproducibility of the measurements and indicated that no permanent deformation of the elastic fiber had occurred. The slope (dF/dz) of the curve in Fig. 3C was used to calculate Young's modulus. During the AFM manipulation, it became clear that the AFM cantilever was able to laterally move elastic fibers on the glass substrate. Therefore, elastic fibers were assumed to be supported, instead of being fixed at the two ends of the channel. Young's modulus of the elastic fibers can then be described by the model of bending isotropic materials, using the expression [36]:

$$E = \frac{l^3}{48I} \times \frac{dF}{dz} \tag{3}$$

In which I is the moment of inertia, equal to $\pi R^4/4$ (elastic fibers were considered a rod with a circular cross-section with radius R), l

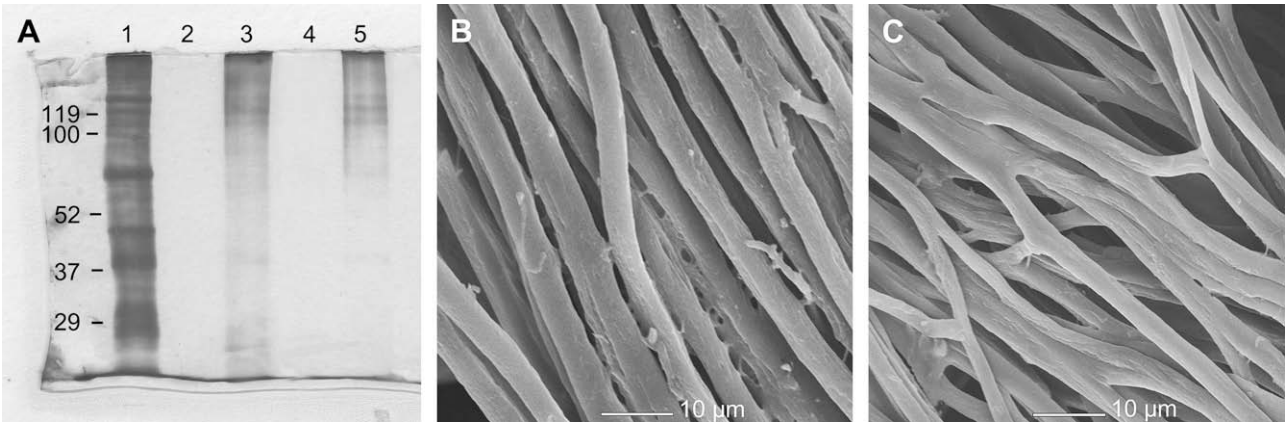

Fig. 1. (A) Gel electrophoresis of purified elastic fiber preparations. Note that, compared to crude *Ligamentum nuchae* (lane 1, 100 μg), purified elastic fibers devoid of fibrillin–microfibrils (lane 2, 100 μg, Method I), or containing fibrillin–microfibrils (lane 4, 100 μg, Method II) did not contain any visible protein bands that indicate contamination or elastin breakdown. Elastic fiber preparations before purification with method I (lane 3, 100 μg) or method II (lane 5, 100 μg still contained some protein bands, indicating that methods I and II successfully removed the contaminations from the preparations. (B) SEM images of elastic fiber preparations after purification using method I (B) and method II (C) (Bar = 10 μm). Note the smooth and intact surface of the elastic fibers.

is the length of the elastic fiber spanning the channel, and *dF/dz* is the slope of the force versus displacement curve obtained from bending experiments of the two elastic fiber preparations.

The diameter of all the tested elastic fiber preparations was determined using SEM imaging of dry fibers. However, during the micromechanical bending test, the glass substrate containing the elastic fibers was immersed in water. This may lead to swelling of the elastic fibers, thereby affecting the diameter. Therefore, the diameters of elastic fibers in the dry and in the hydrated state were estimated by environmental SEM imaging under high (5.4 Torr) and very low (0.6 Torr) water pressure (Fig. 4). SEM images made at high water pressure can be used to determine the dimensions of fully hydrated elastic fibers. By measuring the diameters of a large number of elastic fibers, the diameters of hydrated elastic fibers were found to be 1.1 times larger than the diameters of dry fibers.

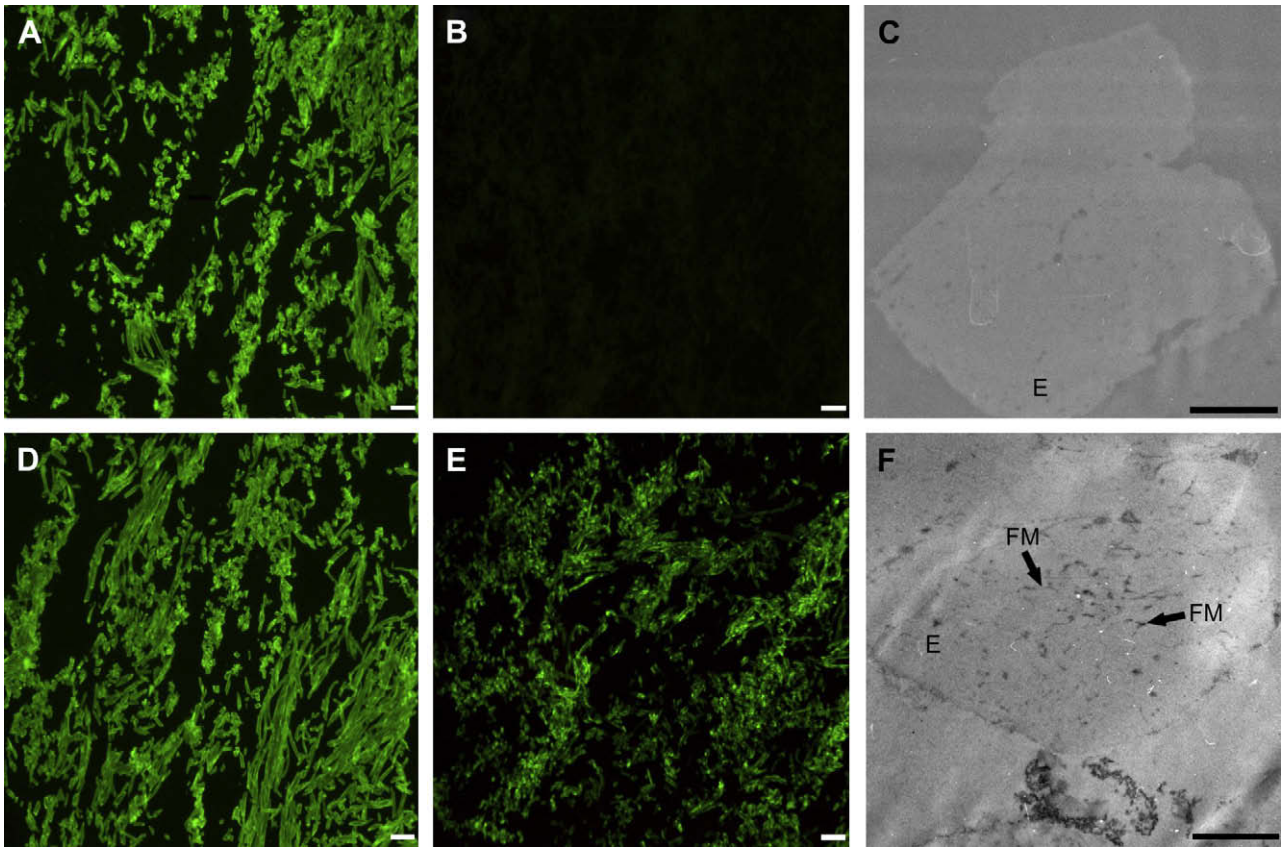

Fig. 2. A,B: Elastic fibers devoid of fibrillin–microfibrils (Method I) immunostained for elastin (A) and fibrillin-1 (B). D,E: Elastic fibers containing fibrillin–microfibrils (Method II) immunostained for elastin (D) and fibrillin-1 (E). Note that in both preparations elastin was abundantly present, whereas fibrillin-1 was only detectable in elastic fibers purified by method II. (Bar = 50 μm) C, F: TEM images of elastic fiber preparations. Note that fibrillin–microfibrils, recognizable as dark, dots/filamentous structures, were only detected in elastic fibers purified by method II (F). *E* = elastin, FM = fibrillin–microfibrils (Bar = 1 μm).

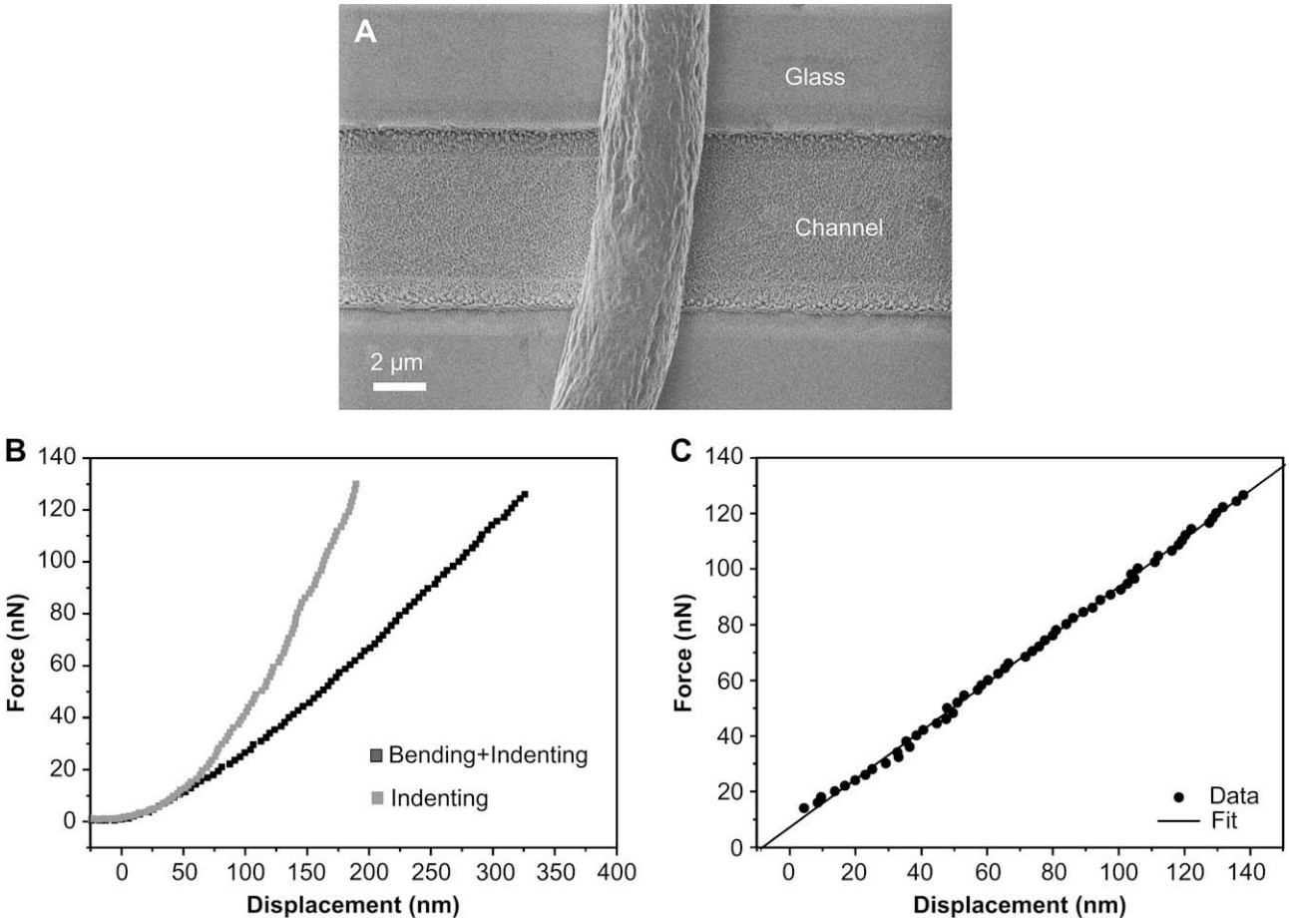

Fig. 3. (A) SEM image of an elastic fiber spanning a micro-channel in the glass substrate. (B) Force versus displacement curves obtained from bending an elastic fiber immersed in water at the middle point of the channel (black squares) and indenting the same elastic fiber on the glass substrate (gray squares). (C) Force versus displacement only representing the bending of the fiber obtained after subtracting for each force the displacement from local indentation.

Elastic fibers devoid of fibrillin–microfibrils had an average Young's modulus of 0.79 ± 0.17 MPa (mean diameter 3.9 ± 0.5 μm (±S.D.)) and elastic fibers containing fibrillin–microfibrils had an average Young's modulus of 0.90 ± 0.23 MPa (mean diameter 4.3 ± 1.1 μm (±S.D.)). Statistically this difference was not significant.

Young's moduli of single elastic fibers ranged between 0.3 and 1.5 MPa, which are comparable to the range stated in literature for single elastic fibers and tissues [18]. The mechanical properties of single elastic fibers from bovine *ligamentum nuchae* were studied, for the first time, by Aaron et al. [7]. Using a microtest apparatus it was shown that Young's modulus of a single elastic fiber is in the

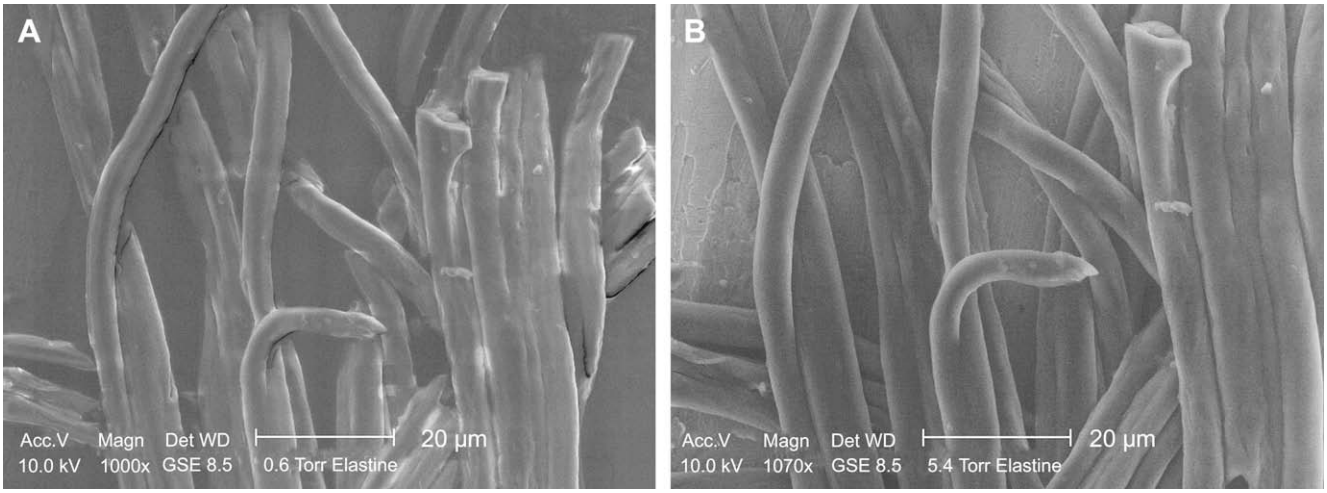

Fig. 4. SEM images of elastic fibers devoid of fibrillin–microfibrils in dry state (0.6 Torr water pressure) (A) and in hydrated state (5.4 Torr water pressure) (B). Note the small increase in the diameter of hydrated elastic fibers as compared to dry fibers.

range of 0.4–1.2 MPa. From macro-mechanical tests on elastin-rich tissue strips, elastic fibers of purified dog or sheep aorta, Young's moduli in the range of 0.13–0.65 MPa were determined [5]. Young's moduli between 0.1 and 0.8 MPa were obtained for elastic fibers in strips of purified pig aorta [6]. The fact that Young's moduli derived from our micromechanical AFM bending test are comparable to the macrotests/microtests of elastin-rich tissue strips/single elastic fibers indicate that the purification procedure did not affect the mechanical properties of the elastic fibers. Although the value is well within the range reported in literature, the full range for the value of Young's modulus, as determined from our measurements, was considerable (0.3–1.5 MPa). This range probably resulted from the assumption that elastic fibers were circular in cross-section, as seen in Eq. (3). As reported previously [32], SEM imaging indicates that some elastic fibers have an irregular cross-sectional area. Interestingly, no significant differences in the values of Young's modulus for the purified elastic fibers devoid of or containing fibrillin–microfibrils was found from our measurements. This result suggests that fibrillin–microfibrils do not influence the modulus of elastic fibers.

3.3. Fibrillin–microfibril preparations

In order to better explain the obtained results on Young's modulus for elastic fibers and to provide more insight in the mechanical properties of fibrillin–microfibrils, isolated fibrillin–microfibrils were prepared for micromechanical tests.

Isolated fibrillin–microfibrils deposited on a glass substrate were imaged by AFM (Fig. 5). As reported previously [37], AFM images displayed the typical "beads-on-a-string" structure for fibrillin–microfibrils (Fig. 5A and B). A distance between two beads of 65 ± 7 nm was determined from the images (Fig. 5C).

3.4. Mechanical properties of fibrillin–microfibrils

Because fibrillin–microfibrils are three orders of magnitude smaller than elastic fibers, poly(methyl methacrylate) (PMMA) coated glass substrates with nano-channels in PMMA of 100–200 nm in width, instead of 5–10 μm, were at first prepared. A suspension of fibrillin–microfibrils was contacted with the PMMA substrate containing the nano-channels. After drying, the substrate was washed with demineralised water and subsequently dried at ambient conditions. The PMMA substrate was then subjected to tapping mode AFM imaging. However, AFM images at different positions of the substrates showed that the fibrillin–microfibrils adhered to the bottom of the channel, instead of spanning the nano-channels. Therefore, micromechanical AFM bending tests could not be performed. Efforts were made to make the surface either hydrophilic by oxygen plasma treatment or positively charged by coating a layer of positively charged protein. Changing the surface properties of PMMA, however, did not promote the spanning of the fibrillin–microfibrils over the channels.

Using high concentrations of fibrillin–microfibrils to deposit the microfibrils onto the glass substrate, enabled the formation of microfibril layers (Fig. 6A) with thicknesses of ~60–100 nm. AFM nano-indentation tests of fibrillin–microfibrils were performed at several locations by approaching the AFM tip to the layered surface until a cantilever deflection was observed. A plot of the cantilever deflection versus the piezo movement in the z-direction was recorded for each indentation, and converted to a force versus indentation curve using Eqs. (1) and (2). A typical force versus indentation curve from nano-indentation of fibrillin–microfibrils is depicted (Fig. 6B). No difference was found in the force versus displacement curve after indenting multiple times at the same position, which ensured the reproducibility of the measurements and indicated that no permanent deformation of the fibrillin–microfibrils had occurred.

AFM nano-indentation tests have been used to determine Young's modulus of different biological samples [38,39] using the theory of Hertz [40] and the mechanics of Sneddon [41]. The relationship between force and indentation is influenced by the geometry of the AFM tip. In this study, the radius of the tip was ~20 nm, which was in the same order as the indentation depth. Therefore, the tip can be assumed to be parabolic with a radius of curvature R at the apex. The force applied on the cantilever (F) as a function of the indentation (x) can then be described using the following expression:

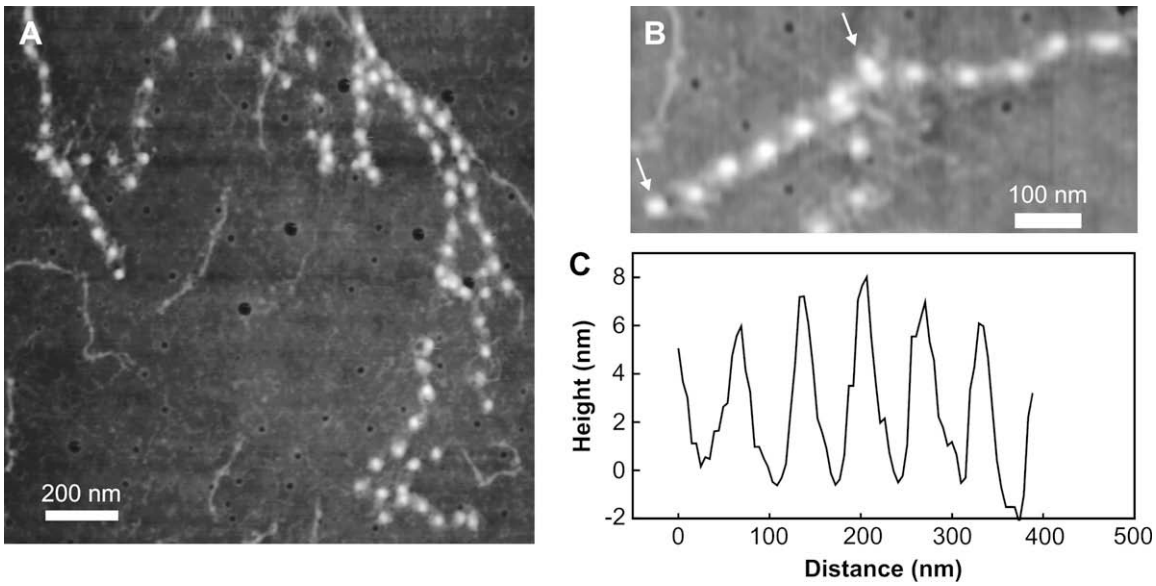

Fig. 5. (A) Tapping mode atomic force microscopy (AFM) height image of fibrillin–microfibrils deposited on a glass surface. (B) Zoom in of tapping mode AFM height image of fibrillin–microfibrils. Note the typical fibrillin–microfibrils beads-on-a-string appearance. (C) Line scans along a fibrillin–microfibril. 6 repeats are shown as indicated by the arrows in image B. The mean distance between the beads was calculated to be 65 ± 7 nm.

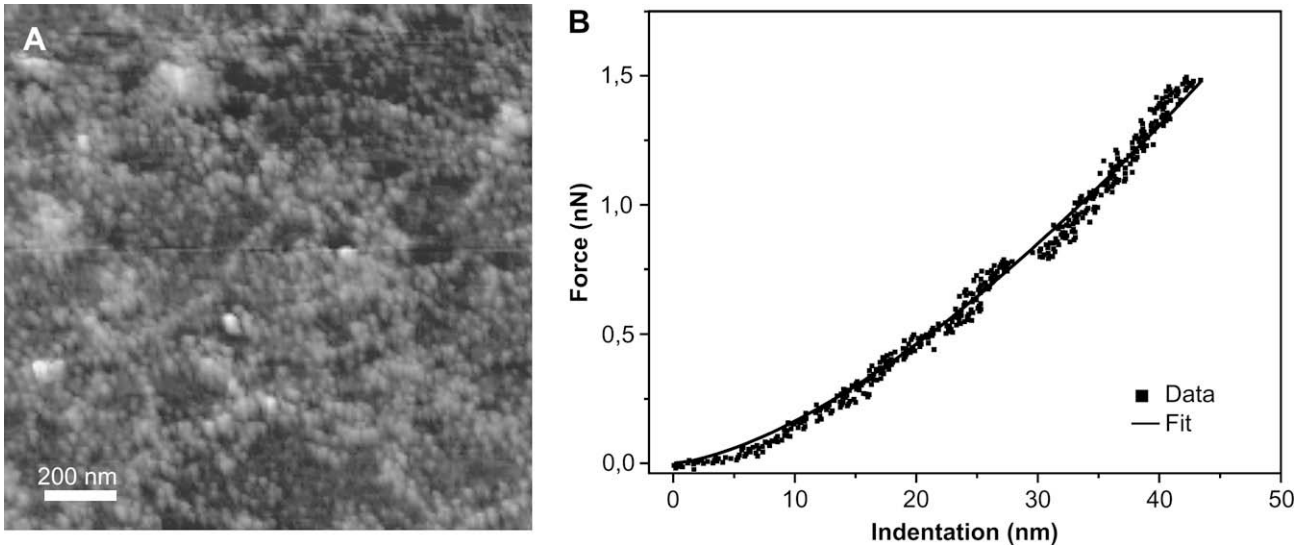

Fig. 6. (A) Contact mode AFM height image of fibrillin–microfibrils layers deposited on a glass surface (Bar = 200 nm). (B) Force versus indentation curves obtained from nano-indentation of fibrillin–microfibrils layers. A relative Young's modulus (E^*) of 0.86 MPa was calculated from fitting the experimental data to Eq. (4).

$$F = \frac{4\sqrt{R}}{3}E^* x^{1.5} \tag{4}$$

where E^* is the relative Young's modulus, defined as:

$$\frac{1}{E^*} = \frac{1-\upsilon_{tip}^2}{E_{tip}} + \frac{1-\upsilon_{sample}^2}{E_{sample}} \tag{5}$$

in which υ_{sample} and υ_{tip} are the Poisson ratio of respectively the sample and the tip. The experimental data of the force versus indentation curve could be fitted with Eq. (4) (Fig. 6B). An average E^* of 0.74 ± 0.17 MPa (±S.E.M.) was calculated from multiple force versus indentation curves obtained from nano-indentation at different locations on the sample. Young's modulus of the AFM tip (~200 GPa) is much higher than Young's modulus of the fibrillin–microfibrils in the hydrated state, therefore the $1/E^*$ is further simplified to:

$$\frac{1}{E^*} \approx \frac{1-\upsilon_{sample}^2}{E_{sample}} \tag{6}$$

Using a typical Poisson ratio of 0–0.5 for elastic materials, Young's modulus (E_{sample}) of fibrillin–microfibrils was estimated to be in the range of 0.56 ± 0.12–0.74 ± 0.17 MPa (± S.E.M.).

It has to be considered that there are still some limitations in the method, influencing the accuracy of the determined Young's modulus. For example, in the model the sample and the tip surface were assumed to be smooth, however, in practice they are usually rough. This uncertainty of the contact area will influence the measurements and can lead to deviations in the order of a few percent [42]. The obtained value was still comparable to Young's moduli estimated for vertebrate or invertebrate fibrillin–microfibrillar networks. The invertebrate microfibrillar network in abdominal lobster aorta has a modulus of ~1.06 MPa [19]. Young's modulus of fibrillin–microfibrils isolated from sea cucumber dermis is approximately 0.2 MPa [20], whereas, the microfibrillar network in jellyfish has an estimated Young's modulus of 0.9 MPa [21]. In vertebrates, Young's modulus of bovine zonular filaments, a structure solely composed of fibrillin–microfibrils, is in the range of 0.19–1.88 MPa [22–24,43].

The current study was designed to determine the role of fibrillin–microfibrils in the mechanical properties of a single elastic fiber. Highly purified elastic fibers, devoid of or containing fibrillin–microfibrils, were extracted from equine *ligamentum nuchae* and subjected to micromechanical AFM bending tests in order to determine Young's modulus. It has to be highlighted that, compared to macro-mechanical tests, AFM is a very accurate method for determining the mechanical properties of micro- and nano-sized materials [44,45]. The determined Young's moduli for single elastic fibers devoid of or containing fibrillin–microfibrils were not significantly different, indicating that fibrillin–microfibrils do not influence the mechanical properties of a single elastic fiber from equine *ligamentum nuchae*. As presented in our results, fibrillin–microfibrils had Young's modulus similar to that of elastic fibers, which can be the reason for the above finding.

Recently, Sherrat et al. used a molecular combing technique to determine Young's modulus of fibrillin–microfibrils isolated from bovine zonular filaments [25]. Young's modulus of 78–96 MPa was determined, a value nearly two orders of magnitude higher than Young's moduli reported in literature for microfibrillar networks as well as the values determined by us for isolated fibrillin–microfibrils. The authors imply that individual fibrillin–microfibrils act as relatively stiff elastic polymers, reinforcing the elastic fibers. However, our direct measurements on the mechanical properties of single elastic fibers devoid of or containing fibrillin–microfibrils did not show a reinforcing effect of these microfibrils. Recent published work by Megill et al. gives an explanation for this paradox [21]. The authors suggest that the mechanical behavior of fibrillin–microfibrils must be fitted by a J-shaped model, instead of the linear model that is derived from the molecular combing experiments by Sherrat et al. Based on reinterpretation of the molecular combing experiments, Megill et al. suggest Young's modulus of 1 MPa for fibrillin–microfibrils, a value that is in the range with our data. Taken all three comments into account, we suggest that fibrillin–microfibrils have Young's moduli in the range of 0.56–0.74 MPa.

4. Conclusions

An AFM-based mechanical technique was applied to study the micro-scale mechanical behavior of single elastic fibers and fibrillin–microfibrils. Highly purified and intact elastic fibers, devoid of or containing fibrillin–microfibrils, were successfully isolated using chemical and enzymatic methods. As determined from micromechanical

bending tests, Young's moduli of single elastic fibers were in the range of 0.3–1.5 MPa. Young's moduli for purified elastic fibers were in the same range as those for elastic fiber-rich tissues. Young's modulus of single elastic fibers was not significantly affected by the absence or presence of fibrillin–microfibrils. Fibrillin–microfibrils have Young's modulus in the range of 0.56–0.74 MPa as determined with nano-indentation tests, which is comparable with Young's modulus of elastic fibers. It is concluded that fibrillin–microfibrils do not significantly influence the mechanical properties of single vertebrate elastic fibers.

Acknowledgements

The authors wish to thank the Department of Pathology, Faculty of Veterinary Medicine, Utrecht University, The Netherlands for providing equine *ligamentum nuchae*.

This research is financially supported by the Softlink program of ZonMw. Project number: 01SL056 and by the Canadian Institutes of Health Research Project number: MOP-68836 to Dieter Reinhardt.

References

[1] Rosenbloom J, Abrams WR, Mecham R. Extracellular matrix 4: the elastic fiber. FASEB J 1993;7:1208–18.
[2] Kielty CM, Shuttleworth CA. Fibrillin-containing microfibrils: structure and function in health and disease. Int J Biochem Cell Biol 1995;27:747–60.
[3] Sakai LY, Keene DR, Engvall E. Fibrillin, a new 350-kD glycoprotein, is a component of extracellular microfibrils. J Cell Biol 1986;103:2499–509.
[4] Sherratt MJ, Wess TJ, Baldock C, Ashworth JL, Purslow PP, Shuttleworth CA, et al. Fibrillin-rich microfibrils of the extracellular matrix: ultrastructure and assembly. Micron 2001;32:185–200.
[5] Sherebrin MH. Mechanical anisotropy of purified elastin from the thoracic aorta of dog and sheep. Can J Physiol Pharmacol 1983;61:539–45.
[6] Lillie MA, David GJ, Gosline JM. Mechanical role of elastin-associated microfibrils in pig aortic elastic tissue. Connect Tissue Res 1998;37:121–41.
[7] Aaron BB, Gosline JM. Elastin as a random-network elastomer – a mechanical and optical analysis of single elastin fibers. Biopolymers 1981;20:1247–60.
[8] Kielty CM, Sherratt MJ, Shuttleworth CA. Elastic fibres. J Cell Sci 2002;115:2817–28.
[9] Gibson MA, Hughes JL, Fanning JC, Cleary EG. The major antigen of elastin-associated microfibrils is a 31-kDa glycoprotein. J Biol Chem 1986;261:1429–36.
[10] Gibson MA, Kumaratilake JS, Cleary EG. The protein-components of the 12-nanometer microfibrils of elastic and nonelastic tissues. J Biol Chem 1989;264:4590–8.
[11] Gibson MA, Hatzinikolas G, Kumaratilake JS, Sandberg LB, Nicholl JK, Sutherland GR. Further characterization of proteins associated with elastic fiber microfibrils including the molecular cloning of MAGP-2 (MP25). J Biol Chem 1996;271:1096–103.
[12] Bressan GM, Dagagordini D, Colombatti A, Castellani I, Marigo V, Volpin D. Emilin, a component of elastic fibers preferentially located at the elastin–microfibrils interface. J Cell Biol 1993;121:201–12.
[13] Colombatti A, Doliana R, Bot S, Canton A, Mongiat M, Mungiguerra, et al. The EMILIN protein family. Matrix Biol 2000;19:289–301.
[14] Doliana R, Mongiat M, Bucciotti F, Giacomello E, Deutzmann R, Volpin D, et al. EMILIN, a component of the elastic fiber and a new member of the C1q/tumor necrosis factor superfamily of proteins. J Biol Chem 1999;74:16773–81.
[15] Isogai Z, Ono RN, Ushiro S, Keene DR, Chen Y, Mazzieri R, et al. Latent transforming growth factor beta-binding protein 1 interacts with fibrillin and is a microfibril-associated protein. J Biol Chem 2003;278:2750–7.
[16] Oklu R, Hesketh R. The latent transforming growth factor beta binding protein (LTBP) family. Biochem J 2000;352:601–10.
[17] Sinha S, Nevett C, Shuttleworth CA, Kielty CM. Cellular and extracellular biology of the latent transforming growth factor-beta binding proteins. Matrix Biol 1998;17:529–45.
[18] Faury G. Function–structure relationship of elastic arteries in evolution: from microfibrils to elastin and elastic fibres. Pathol Biol 2001;49:310–25.
[19] McConnell CJ, Wright GM, DeMont ME. The modulus of elasticity of lobster aorta microfibrils. Experientia 1996;52:918–21.
[20] Thurmond FA, Trotter JA. Morphology and biomechanics of the microfibrillar network of sea cucumber dermis. J Exp Biol 1996;199:1817–28.
[21] Megill WM, Gosline JM, Blake RW. The modulus of elasticity of fibrillin-containing elastic fibres in the mesoglea of the hydromedusa *Pollyorchis penicillatus*. J Exp Biol 2005;208:3819–34.
[22] Wright DW, McDaniels CN, Swasdison S, Accavitti MA, Mayne PM, Mayne R. Immunization with undenatured bovine zonular fibrils results in monoclonal antibodies to fibrillin. Matrix Biol 1994;14:41–9.
[23] Wess TJ, Purslow PP, Sherratt MJ, Ashworth J, Shuttleworth CA, Kielty CM. Calcium determines the supramolecular organization of fibrillin-rich microfibrils. J Cell Biol 1998;141:829–37.
[24] Ziebarth NM, Wojcikiewicz EP, Manns F, Moy VT, Parel JM. Atomic force microscopy measurements of lens elasticity in monkey eyes. Mol Vis 2007;13:504–10.
[25] Sherratt MJ, Baldock C, Haston JL, Holmes DF, Jones CJP, Shuttleworth CA, et al. Fibrillin microfibrils are stiff reinforcing fibres in compliant tissues. J Mol Biol 2003;332:183–93.
[26] Buttafoco L, Engbers-Buijtenhuijs P, Poot AA, Dijkstra PJ, Daamen WF, van Kuppevelt TH, et al. First steps towards tissue engineering of small-diameter blood vessels: preparation of flat scaffolds of collagen and elastin by means of freeze drying. J Biomed Mater Res B 2006;77:357–68.
[27] Buttafoco L, Kolkman NG, Engbers-Buijtenhuijs P, Poot AA, Dijkstra PJ, Vermes I, et al. Electrospinning of collagen and elastin for tissue engineering applications. Biomaterials 2006;27:724–34.
[28] Daamen WF, van Morerkerk HTB, Hafmans T, Buttafoco L, Poot AA, Veerkamp JH, et al. Preparation and evaluation of molecularly-defined collagen–elastin–glycosaminoglycan scaffolds for tissue engineering. Biomaterials 2003;24:4001–9.
[29] Daamen WF, Nillesen STM, Hafmans T, Veerkamp JH, van Luyn MJA, van Kuppevelt TH. Tissue response of defined collagen–elastin scaffolds in young and adult rats with special attention to calcification. Biomaterials 2005;26:81–92.
[30] Yang L, van der Werf KO, Koopman BFJM, Subramaniam V, Bennink ML, Dijkstra PJ, et al. Micromechanical bending of single collagen fibrils using atomic force microscopy. J Biomed Mater Res A 2007;82:160–8.
[31] Daamen WF, Hafmans T, Veerkamp JH, van Kuppevelt TH. Comparison of five procedures for the purification of insoluble elastin. Biomaterials 2001;22:1997–2005.
[32] Daamen WF, Hafmans T, Veerkamp JH, van Kuppevelt TH. Isolation of intact elastin fibers devoid of microfibrils. Tissue Eng 2005;11:1168–76.
[33] Tiedemann K, Bätge B, Müller PK, Reinhardt DP. Interactions of fibrillin-1 with heparin/heparan sulfate, implications for microfibrillar assembly. J Biol Chem 2001;276:36035–42.
[34] Torii A, Sasaki M, Hane K, Okuma S. A method for determining the spring constant of cantilevers for atomic force microscopy. Meas Sci Technol 1996;7:179–84.
[35] Kielty CM, Shuttleworth CA. Abnormal fibrillin assembly by dermal fibroblasts from two patients with Marfan syndrome. J Cell Biol 1994;124:997–1004.
[36] Gere JM, Timoshenko SP. Mechanics of materials. Cheltenham: Stanley Thornes Ltd.; 1999.
[37] Kielty CM, Cummings C, Whittaker SP, Shuttleworth CA, Grant ME. Isolation and ultrastructural analysis of microfibrillar structures from foetal bovine elastic tissues. Relative abundance and supramolecular architecture of type VI collagen assemblies and fibrillin. J Cell Sci 1991;99:797–807.
[38] Vinckier A, Semenza G. Measuring elasticity of biological materials by atomic force microscopy. FEBS Lett 1998;430:12–6.
[39] Radmacher M, Fritz M, Cleveland JP, Walters DA, Hansma PK. Imaging adhesion forces and elasticity of lysozyme adsorbed on mica with the atomic force microscope. Langmuir 1994;10:3809–14.
[40] Timoschenko S, Goodier J. Theory of elasticity. 3rd ed. New York: McGraw-Hill; 1987.
[41] Sneddon IN. The relation between load and penetration in the axisymmetric boussinesq problem for a punch of arbitrary profile. Int J Eng Sci 1965;3:47–57.
[42] Bouzakis KD, Michailidis N, Hadjiyiannis S, Skordaris G, Erkens G. The effect of specimen roughness and indenter tip geometry on the determination accuracy of thin hard coatings stress–strain laws by nanoindentation. Mater Charact 2002;49:149–56.
[43] Wright DM, Duance VC, Wess TJ, Kielty CM, Purslow PP. The supramolecular organisation of fibrillin-rich microfibrils determines the mechanical properties of bovine zonular filaments. J Exp Biol 1999;202:3011–20.
[44] Jacot JG, Dianis S, Schnall J, Wong JY. A simple microindentation technique for mapping the microscale compliance of soft hydrated materials and tissues. J Biomed Mater Res A 2006;79:485–94.
[45] Matsumoto T, Abe H, Ohashi T, Kato Y, Sato M. Local elastic modulus of atherosclerotic lesions of rabbit thoracic aortas measured by pipette aspiration method. Physiol Meas 2002;23:635–48.